Aalto University

Aaltodoc
OPEN ACCESS

This is an electronic reprint of the original article.
This reprint may differ from the original in pagination and typographic detail.

Author(s): M. W. Ray, E. Ruokokoski, K. Tiurev, M. Möttönen, and D. S. Hall

Title: Observation of Dirac monopoles in a synthetic magnetic field

Year: 2015

Version: Post print

Please cite the original version:

M. W. Ray, E. Ruokokoski, K. Tiurev, M. Möttönen, and D. S. Hall. Observation of Isolated Monopoles in a Quantum Field. Science, 348, 6234, May 2015. DOI: 10.1126/science.1258289

Rights: © The American Association for the Advancement of Science (AAAS). Reprinted with permission.

This publication is included in the electronic version of the article dissertation:
Ruokokoski, Emmi. Magnetic-Monopole Analogues and Topological Textures in Dilute Bose-Einstein Condensates.
Aalto University publication series DOCTORAL DISSERTATIONS, 81/2015.

All material supplied via Aaltodoc is protected by copyright and other intellectual property rights, and duplication or sale of all or part of any of the repository collections is not permitted, except that material may be duplicated by you for your research use or educational purposes in electronic or print form. You must obtain permission for any other use. Electronic or print copies may not be offered, whether for sale or otherwise to anyone who is not an authorised user.

Observation of Isolated Monopoles in a Quantum Field

M. W. Ray, [1,†] E. Ruokokoski, [2] K. Tiurev, [2] M. Möttönen, [2,3*] D. S. Hall [1]

[1]Department of Physics and Astronomy, Amherst College, Amherst, MA 01002-5000, USA
[2]QCD Labs, COMP Centre of Excellence, Department of Applied Physics, Aalto University, P.O. Box 13500, FI–00076 Aalto, Finland
[3]Low Temperature Laboratory (OVLL), Aalto University, P.O. Box 13500, FI-00076 Aalto, Finland
[†]Present address: Department of Physics and Astronomy, Union College, Schenectady, NY 12308, USA
[*]To whom correspondence should be addressed; E-mail: mikko.mottonen@aalto.fi.

Topological defects play important roles throughout nature, appearing in contexts as diverse as cosmology, particle physics, superfluidity, liquid crystals, and metallurgy. Point defects can arise naturally as magnetic monopoles resulting from symmetry breaking in grand unified field theories. Here, we experimentally demonstrate the creation and detection of quantum-mechanical analogues of such monopoles in a spin-1 Bose-Einstein condensate. The defects, which are stable on the time scale of our experiments, are identified from spin-resolved images of the condensate density profile that exhibit a characteristic dependence on the choice of quantization axis. Our observations lay the foundation for experimental studies of the dynamics and stability of topological point defects in quantum systems.

Two structures are topologically equivalent if they can be continuously transformed into

one another [1, 2], such as the letters ‘O’ and ‘P’. Topological defects exist in a physical system if its state is not topologically equivalent to its ground state. Such defects can only decay or disappear in globally non-trivial transformations, rendering them long-lived and ubiquitous in the universe.

Line defects are among the most common topological structures. In classical physics, for example, dislocations in a crystal lattice [3] can determine the strength and hardness of materials. In quantum physics, a line defect in a complex-valued order parameter is accompanied by a phase winding of an integer multiple of 2π. These quantized vortices are regarded as the hallmark of superfluidity [4, 5] and constitute a versatile tool in the study of quantum physics. In contrast, the roles played by point defects in three-dimensional superfluids and superconductors remain less explored experimentally, although related objects such as skyrmion solitons and boojums at domain interfaces have been observed [6, 7, 8, 9].

Homotopy theory [2, 10] is a mathematical tool that classifies topological point defects by the behavior of the order parameter on closed surfaces. Evaluation of the second homotopy group reveals whether point defects can occur. Nematic liquid crystals [11] and colloids [12] are examples of classical systems for which the second homotopy group is non-trivial and point defects have been observed [see also Ref. [13]]. Quantum systems described by multi-dimensional fields are also predicted to support point defects as stable elementary particles [2]. The magnetic monopole [14, 15] that emerges under broken symmetry in grand unified gauge theories [16] is one such example. Importantly for our work, the polar phase of a spin-1 BEC permits the existence of topological point defects in the quantum-mechanical order parameter [17, 18]. Although these defects are not elementary particles, they are analogous

quantum objects often referred to as monopoles.

We experimentally create a topological point defect in the spin-1 order parameter of a ^{87}Rb BEC using a method originally suggested in Ref. [19] and used to create Dirac monopoles in a ferromagnetic BEC in Ref. [20] [see related work in Ref. [21]]. The key technical difference as compared with Ref. [20] is that the condensate is initialized in its polar phase. This seemingly minor modification leads to a topological excitation with properties that are fundamentally different from those of the recently observed Dirac monopole. The Dirac monopole is not a point-like topological defect in the order parameter, as the second homotopy group of the ferromagnetic phase contains only the identity element [22]. Consequently, Dirac monopoles are attached to at least one terminating nodal line [23], which renders the energetics and dynamics of the excitation similar to those of vortices. No such nodal line is attached to the point defect structure we create here in the order parameter field, and hence we shall refer to it throughout this report as an isolated monopole.

A spin-1 condensate can be described by the order parameter $\Phi(\mathbf{r}) = \sqrt{n(\mathbf{r})}e^{i\phi(\mathbf{r})}\zeta(\mathbf{r})$, where n is the particle density, ϕ is the scalar phase, and the spinor is represented by a normalized complex-valued vector $\zeta = (\zeta_{+1}\ \zeta_0\ \zeta_{-1})^T$. Here $\zeta_m = \langle m|\zeta\rangle$ is the mth spinor component along the quantization axis z. The most general polar order parameter, for which the local spin vanishes, is given by

$$\Phi = \frac{\sqrt{n}e^{i\phi}}{\sqrt{2}}\begin{pmatrix} -e^{-i\alpha}\sin\beta \\ \sqrt{2}\cos\beta \\ e^{i\alpha}\sin\beta \end{pmatrix} = \frac{\sqrt{n}e^{i\phi}}{\sqrt{2}}\begin{pmatrix} -d_x + id_y \\ \sqrt{2}d_z \\ d_x + id_y \end{pmatrix}, \quad (1)$$

where the Euler angles $\beta(\mathbf{r})$ and $\alpha(\mathbf{r})$ refer to the spin rotation of a spinor $(0\ 1\ 0)^T$ about the y- and z-axis, respectively, and $\hat{\mathbf{d}}$ is a three-dimensional real-valued unit vector

field known as the nematic vector. Equation 1 shows that the polar spin-1 condensate is simply described by the mean-field order parameter $\mathbf{\Psi}(\mathbf{r}) = \sqrt{n(\mathbf{r})}e^{i\phi(\mathbf{r})}\hat{\mathbf{d}}(\mathbf{r})$, with its topological properties determined by the factor $e^{i\phi(\mathbf{r})}\hat{\mathbf{d}}(\mathbf{r})$ (supplementary online text). Note that any unitary spin rotation imposed on the order parameter in Eq. 1 corresponds to an identical rotation of $\hat{\mathbf{d}}$. Thus the nematic vector $\hat{\mathbf{d}}$ follows adiabatic changes in the external magnetic field, much as the direction of the spin follows the field in the ferromagnetic case.

The initial atom number in the optically-trapped ^{87}Rb BEC is $N \approx 2.1\times10^5$ with calculated radial and axial Thomas-Fermi radii $R = 7.2\ \mu$m and $Z = 5.4\ \mu$m, respectively, and corresponding optical trapping frequencies $\omega_r \approx 2\pi\times124$ Hz and $\omega_z \approx 2\pi\times164$ Hz, respectively. The creation process begins with $\hat{\mathbf{d}}$ aligned with a uniform magnetic field $\mathbf{B}_{\rm b}(t) = B_x(t)\hat{\mathbf{x}} + B_y(t)\hat{\mathbf{y}} + B_z(t)\hat{\mathbf{z}}$ [24]. We use $\mathbf{B}_{\rm b}(t) = B_z(t)\hat{\mathbf{z}}$ here, but the experimental results are independent of the choice of direction. A quadrupole magnetic field $\mathbf{B}_{\rm q}(\mathbf{r}) = b_{\rm q}(x\hat{\mathbf{x}} + y\hat{\mathbf{y}} - 2z\hat{\mathbf{z}})$ of strength $b_{\rm q} = 3.7$ G/cm is then introduced; the zero point $\mathbf{r}_0(t) = [-B_x(t)\hat{\mathbf{x}} - B_y(t)\hat{\mathbf{y}} + B_z(t)\hat{\mathbf{z}}/2]/b_{\rm q}$ of the total magnetic field $\mathbf{B}(\mathbf{r},t) = \mathbf{B}_{\rm q}(\mathbf{r}) + \mathbf{B}_{\rm b}(t)$ is initially located well outside the condensate. We then change $\mathbf{B}_{\rm b}$ until $\mathbf{r}_0$ lies near the center of the condensate (Fig. 1A). This 'creation ramp' is carried out nearly adiabatically ($\dot{B}_z = -0.25$ G/s), i.e., $\hat{\mathbf{d}}(\mathbf{r},t) \approx \widehat{\mathbf{B}}(\mathbf{r},t)$, thereby creating the isolated monopole structure in the order-parameter field shown in Fig. 1, B and C. Non-adiabatic excitations and spin-exchange collisions are measured to be relatively small (~10%) for the experimental parameter values employed here.

To select a quantization axis for imaging the monopole structure, we apply a 'projection ramp', in which the magnetic bias field is rapidly increased to $|\mathbf{B}_{\rm b}|/b_{\rm q} \gg R, Z$ along a direction

of our choice, $\hat{\mathbf{z}}_{\mathrm{p}}$, leaving the nematic vector essentially unchanged. Subsequently, the spinor components quantized along this axis, $\langle m_{\mathrm{p}}|\zeta\rangle$, are spatially separated and imaged in both the vertical ($\hat{\mathbf{z}}$) and horizontal ($\hat{\mathbf{y}}$) directions [24]. In Fig. 2, A and D, we show the corresponding experimentally obtained particle densities in the simple case $\hat{\mathbf{z}}_{\mathrm{p}} = -\hat{\mathbf{z}}$. The theory [Eq. 1 with $\hat{\mathbf{d}}(\mathbf{r}, t) = \widehat{\mathbf{B}}_{\mathrm{q}}(\mathbf{r})$] predicts hollow-core vortices of opposite unit circulations in the $m = \pm 1$ components along z, in agreement with the observed density 'holes' in Fig. 2D. The unit phase winding, and the opposite circulations of the two vortices, are experimentally confirmed using interferometric techniques [24] as shown in Figs. S1 and S2. Furthermore, the data in Fig. 2, A and C, are in qualitative agreement with Eq. 1 as the particle density in the $m = 0$ component $n|\zeta_0|^2 \propto d_z^2$ vanishes in the $z = 0$ plane, and the other two components $n|\zeta_{\pm 1}|^2 \propto d_x^2 + d_y^2$ accumulate in its vicinity. This agreement constitutes the primary evidence for the existence of the monopole.

We model the experimental creation and imaging process numerically by solving the full three-dimensional dynamics of the mean-field spinor order parameter from the spin-1 Gross–Pitaevskii equation [19]. Figures 2 and 3 show one-to-one comparisons of the numerically obtained particle density distributions to the experimental results without any free parameters. The good quantitative agreement between the simulations and the experiments reinforces the congruence between the experiments and the results of the analytic theory, thereby providing complementary evidence for the realization of an isolated monopole structure in the order parameter. Discrepancies between the numerical and experimental results, e.g., the density peak in the $m = 0$ component in Fig. 2F, may arise from the experimental noise and imaging technique that are not taken fully into account in the simulations [24].

Identical particle densities to the ones shown in Fig. 2 for our isolated monopole are expected for the topologically equivalent hedgehog monopole structure shown in Fig. 1D, as the only difference between the spinors of the two configurations is the sign of the $m = \pm 1$ components (see Eq. 1 and Fig. 1, C and D). In fact, after the projection ramp $\hat{\mathbf{z}}_\mathrm{p} = \pm\hat{\mathbf{z}}$ the order parameter oscillates between the two configurations because of the 350-kHz Larmor precession of the nematic vector about $\hat{\mathbf{z}}$. Because the other condensate dynamics occur on much longer time scales, the experiment also accurately produces the hedgehog monopole, as confirmed by the numerical simulations shown in Fig. S3.

One characteristic feature of a quantum-mechanical point defect is that arbitrary rotations of a properly chosen coordinate system, $\mathcal{D}$, can be compensated by rotations in the order parameter space, $\widehat{\mathcal{D}}$, and vice versa. We study whether the created point defect has this property by imposing a spin rotation $\widehat{\mathcal{D}}_\mathrm{p}$ on the spin state of the defect $|\zeta\rangle$ such that we choose the direction of the projection ramp, $\hat{\mathbf{z}}_\mathrm{p}$, defined by the coordinate rotation $\left(x_\mathrm{p}, y_\mathrm{p}, z_\mathrm{p}\right) = \mathcal{D}_\mathrm{p}^{-1}(x, y, z)$. The projection of the original spinor onto the new z_p-quantized basis is equal to the projection of the rotated spinor onto the z-quantized basis, i.e., $\langle m_\mathrm{p}|\zeta\rangle = \langle m_\mathrm{p}|\widehat{\mathcal{D}}_\mathrm{p}^{\dagger}\widehat{\mathcal{D}}_\mathrm{p}|\zeta\rangle = \langle m|\widehat{\mathcal{D}}_\mathrm{p}|\zeta\rangle$. Thus the rotational compensation property given above demands that there exists a rotation $\mathcal{D}_\mathrm{v}$ into a new coordinate system $(x_\mathrm{v}, y_\mathrm{v}, z_\mathrm{v}) = \mathcal{D}_\mathrm{v}(x, y, z)$ such that Eq. 1, with (x, y, z) replaced by $(x_\mathrm{v}, y_\mathrm{v}, z_\mathrm{v})$, yields the observed spinor components. Below, we analytically find the new coordinate system for both the hedgehog monopole and our isolated monopole in the case of an arbitrary projection axis, and show matching experimental observations.

The hedgehog monopole is characterized by the nematic vector $\hat{\mathbf{d}}_\mathrm{h} = -\hat{\mathbf{r}}'$, where the

primed coordinates are defined as $(x', y', z') = (x, y, 2z)$. Because the radial vectors in any two rotated coordinate systems coincide, $\hat{\mathbf{r}}'(x'_{\mathrm{p}}, y'_{\mathrm{p}}, z'_{\mathrm{p}}) = \hat{\mathbf{r}}'_{\mathrm{p}}(x'_{\mathrm{p}}, y'_{\mathrm{p}}, z'_{\mathrm{p}})$, we can choose $(x'_{\mathrm{v}}, y'_{\mathrm{v}}, z'_{\mathrm{v}}) = (x'_{\mathrm{p}}, y'_{\mathrm{p}}, z'_{\mathrm{p}})$, i.e., $\mathcal{D}_{\mathrm{v}} = \mathcal{D}_{\mathrm{p}}^{-1}$. Together with Eq. 1, this shows that the vortices in the $m_{\mathrm{p}} = \pm 1$ components of the hedgehog configuration always align with the projection axis $\hat{\mathbf{z}}_{\mathrm{p}}$. To find how the vortices will be oriented in the case of our isolated monopole, we employ the property that the hedgehog monopole is obtained from the isolated monopole configuration by a continuous π-rotation about the z-axis (see Fig. 1, C and D), i.e., $\hat{\mathcal{R}}_z(\pi)|\zeta_{\mathrm{m}}\rangle = |\zeta_{\mathrm{h}}\rangle$ and $\mathcal{R}_z(\pi)\hat{\mathbf{d}}_{\mathrm{m}} = \hat{\mathbf{d}}_{\mathrm{h}}$. By writing the observed spinor component as $\langle m_{\mathrm{p}}|\zeta_{\mathrm{m}}\rangle = \langle m_{\mathrm{p}}|\hat{\mathcal{R}}_z(\pi)^{\dagger}\hat{\mathcal{R}}_z(\pi)|\zeta_{\mathrm{m}}\rangle = \left[\langle m_{\mathrm{p}}|\hat{\mathcal{R}}_z(\pi)^{\dagger}\right]|\zeta_{\mathrm{h}}\rangle$, we find that a proper choice of the new coordinate system is $(x_{\mathrm{v}}, y_{\mathrm{v}}, z_{\mathrm{v}}) = \mathcal{R}_z(\pi)(x_{\mathrm{p}}, y_{\mathrm{p}}, z_{\mathrm{p}})$. Thus the vortices are aligned with $\hat{\mathbf{z}}_{\mathrm{v}} = \mathcal{R}_z(\pi)\hat{\mathbf{z}}_{\mathrm{p}}$.

The isolated monopole (Fig. 1, B and C) is topologically equivalent to the hedgehog structure (Fig. 1D) and has the same topological charge and stability properties. However, the fact that the projection axis and the vortex axis are not always aligned makes the isolated monopole an ideal object to demonstrate that the observed vortices are not technical artifacts of the projection ramp. The corresponding experimental results are shown in Fig. 4. In agreement with the result $\hat{\mathbf{z}}_{\mathrm{v}} = \mathcal{R}_z(\pi)\hat{\mathbf{z}}_{\mathrm{p}}$ derived above, we observe that the two axes, $\hat{\mathbf{z}}_{\mathrm{v}}$ and $\hat{\mathbf{z}}_{\mathrm{p}}$, are parallel when they lie in the xy plane (Fig. 4A), and rotate in opposite directions in the xz plane (Fig. 4B).

Both monopole structures are expected to exhibit an instability toward a formation of a vortex ring [25]. Although this and other instabilities [26, 27] occur slowly enough not to disturb the creation and imaging process (supplementary online text), observation of the resulting

decay dynamics and implementation of a system where they are absent are interesting research directions. Furthermore, studies of the interaction between monopoles and other topological defects, such as domain walls and skyrmions [7], may yield additional insights into high-energy physics and cosmology [28]. A related goal is to create a topological point defect that also generates the synthetic magnetic field of a monopole, thereby combining the scenarios of Dirac [23], ’t Hooft [14] and Polyakov [15]. Finally, the observation of non-Abelian monopoles [29, 30] remains an important goal.

References and Notes

[1] N. D. Mermin, *Rev. Mod. Phys.* **51**, 591 (1979).

[2] M. Nakahara, *Geometry, Topology and Physics* (Taylor & Francis Group, Boca Raton, 2003).

[3] N. W. Ashcroft, N. D. Mermin, *Solid State Physics* (Harcourt College Publishing, Orlando, 1976).

[4] R. J. Donnelly, *Quantized Vortices in Helium II* (Cambridge University Press, Cambridge, 1991).

[5] A. L. Fetter, *Rev. Mod. Phys.* **81**, 647 (2009).

[6] J.-y. Choi, W. J. Kwon, Y.-i. Shin, *Phys. Rev. Lett.* **108**, 035301 (2012).

[7] P. Milde, *et al.*, *Science* **340**, 1076 (2013).

[8] R. Blaauwgeers, *et al.*, *Nature* **404**, 471 (2000).

[9] R. Blaauwgeers, *et al.*, *Phys. Rev. Lett.* **89**, 155301 (2002).

[10] G. Toulouse, M. Kléman, *J. Physique Lett.* **37**, 149 (1976).

[11] I. Chuang, R. Durrer, N. Turok, B. Yurke, *Science* **251**, 1336 (1991).

[12] B. Senyuk, *et al.*, *Nature* **493**, 200 (2013).

[13] S. T. Bramwell, *et al.*, *Nature* **461**, 956 (2009).

[14] G. ’t Hooft, *Nuclear Physics B* **79**, 276 (1974).

[15] A. M. Polyakov, *JETP Letters* **20**, 194 (1974).

[16] J. Preskill, *Ann. Rev. Nucl. Part. Sci.* **34**, 461 (1984).

[17] H. T. C. Stoof, E. Vliegen, U. Al Khawaja, *Phys. Rev. Lett.* **87**, 120407 (2001).

[18] F. Zhou, *Int. J. Mod. Phys. B* **17**, 2643 (2003).

[19] V. Pietilä, M. Möttönen, *Phys. Rev. Lett.* **103**, 030401 (2009).

[20] M. W. Ray, E. Ruokokoski, S. Kandel, M. Möttönen, D. S. Hall, *Nature* **505**, 657 (2014).

[21] J.-y. Choi, S. Kang, S. W. Seo, W. J. Kwon, Y.-i. Shin, *Phys. Rev. Lett.* **111**, 245301 (2013).

[22] Y. Kawaguchi, M. Ueda, *Physics Reports* **520**, 253 (2012).

[23] P. A. M. Dirac, *Proc. R. Soc. Lond. A* **133**, 60 (1931).

[24] Materials and methods are available as supporting materials on Science Online.

[25] J. Ruostekoski, J. R. Anglin, *Phys. Rev. Lett.* **91**, 190402 (2003).

[26] W. Zhang, D. L. Zhou, M.-S. Chang, M. S. Chapman, L. You, *Phys. Rev. Lett.* **95**, 180403 (2005).

[27] L. E. Sadler, J. M. Higbie, S. R. Leslie, M. Vengalattore, D. M. Stamper-Kurn, *Nature* **443**, 312 (2006).

[28] M. O. Borgh, J. Ruostekoski, *Phys. Rev. Lett.* **109**, 015302 (2012).

[29] J. Ruseckas, G. Juzeli u ūnas, P. Öhberg, M. Fleischhauer, *Phys. Rev. Lett.* **95**, 010404 (2005).

[30] V. Pietilä, M. Möttönen, *Phys. Rev. Lett.* **102**, 080403 (2009).

[31] E. A. Burt, *et al.*, *Phys. Rev. Lett.* **79**, 337 (1997).

Acknowledgments:

We acknowledge funding by the National Science Foundation (grant PHY–1205822), by the Academy of Finland through its Centres of Excellence Program (grant no. 251748) and grants (nos 135794 and 272806), Finnish Doctoral Programme in Computational Sciences, and the Magnus Ehrnrooth Foundation. CSC - IT Center for Science Ltd. (Project No. ay2090) and Aalto Science-IT project are acknowledged for computational resources. We thank M. Nakahara and M. Krusius for discussions concerning this work, and N.H. Thomas and S.J. Vickery for experimental assistance. All data used to support the conclusions of this work are presented either in this manuscript or in the Supporting Online Material.

M.W.R. and D.S.H. developed and conducted the experiments and analysed the data. E.R. and K.T. performed the numerical simulations under the guidance of M.M. who provided the initial ideas and suggestions for the experiment. All authors discussed both experimental and theoretical results and commented on the manuscript.

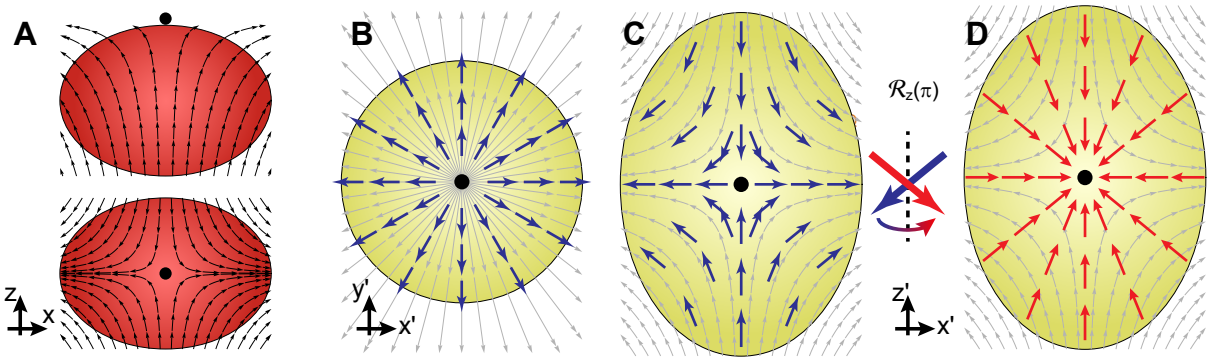

Fig. 1. Schematic representation of the experiment. (**A**) Magnetic field lines as B_z is decreased. The zero-point of the magnetic field is shown as a black dot. (**B**)–(**D**) Cross sections through the condensate in the (**B**) $x'y'$ and (**C**) $x'z'$ planes showing the nematic vector field (thick arrows) defining our isolated monopole structure, which is related to the hedgehog monopole structure (**D**) by a rotation of π about the z'-axis, $\mathcal{R}_z(\pi)$. The primed coordinates are defined as $x' = x$, $y' = y$, and $z' = 2z$, and the gray arrows depict magnetic field lines.

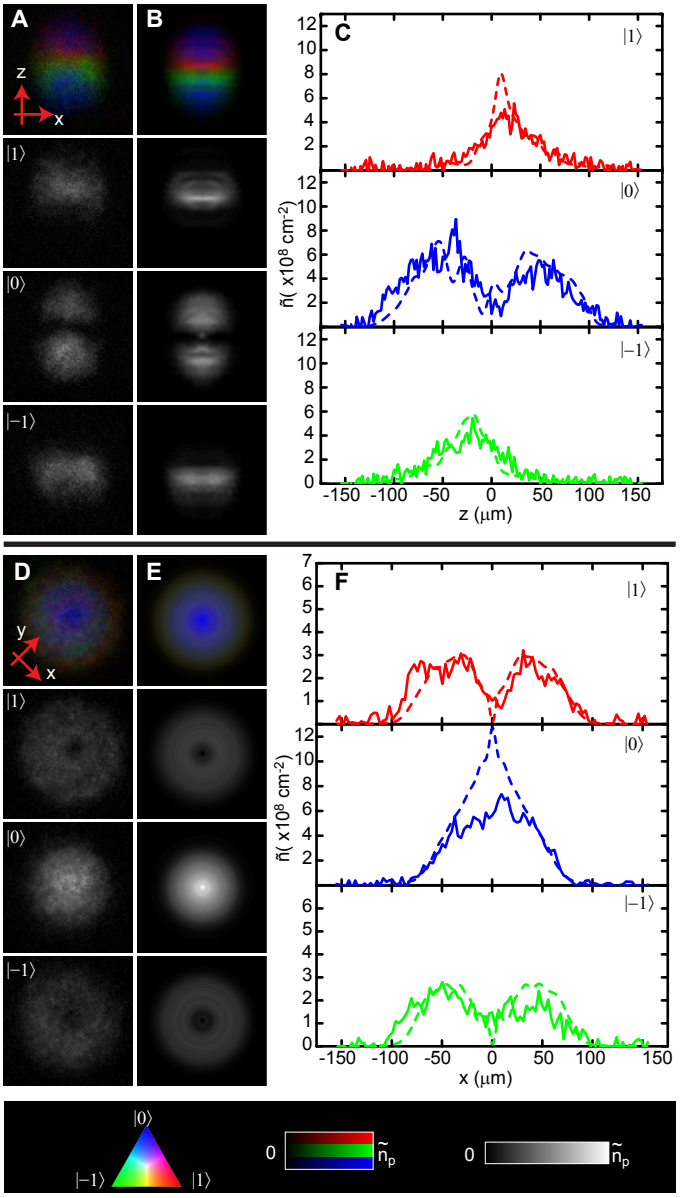

Fig. 2. Experiment compared to numerical simulations following a projection ramp along $-z$. Experimentally obtained images of the condensate were taken along the horizontal (y) axis (**A**), and vertical (z) axis (**D**) and compared to corresponding results of numerical simulations (**B**) and (**E**). In each panel the top image gives a false-color composite, in which the color intensity represents the particle density of each spinor component integrated along the respective imaging axis. The lower three sets of images show the densities for the individual components. (**C**), (**F**) Quantitative comparison of experimental (solid lines) and simulated (dashed lines) column density, $\tilde{n}$, for cross-sections. The field of view is (288×288) $\mu\mathrm{m}^2$ for images along the horizontal axis, and (219×219) $\mu\mathrm{m}^2$ for those along the vertical axis. The peak column density in all images is $\tilde{n}_p = 12.9\times10^8$ cm $^{-2}$.

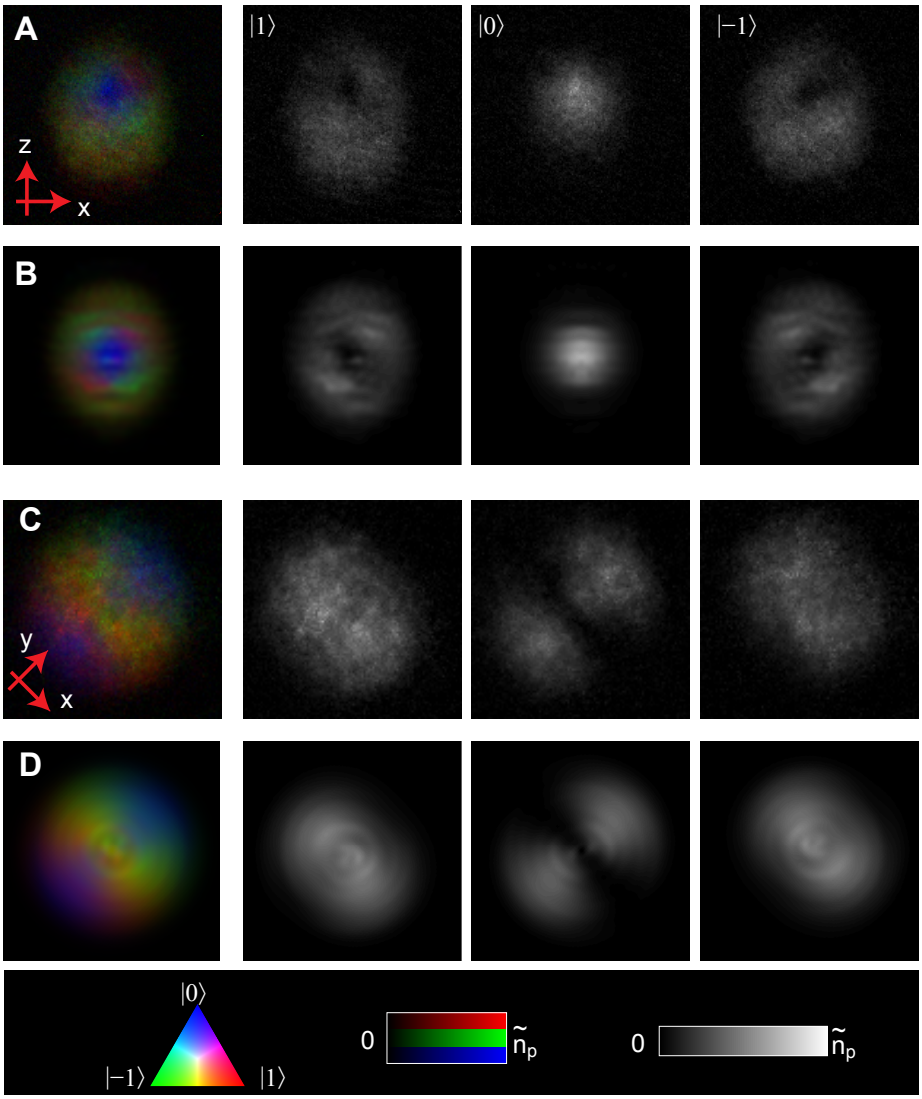

Fig. 3. Experiment compared to numerical simulations following a projection ramp along $-\mathbf{y}$. (A) Experimentally obtained images of the condensate were taken along the horizontal (y) axis and compared to (**B**) results of corresponding numerical simulations. See Fig. 2 for further description. (**C**),(**D**) As above, but for images taken along the vertical (z) axis. The field of view is $(288\times288)\ \mu\mathrm{m}^2$ in panels (**A**) and (**B**), and $(219\times219)\ \mu\mathrm{m}^2$ in panels (**C**) and (**D**). The peak column density is $\tilde{n}_p = 12.9\times10^8$ cm $^{-2}$. Color and intensity scales are given in the bottommost panel.

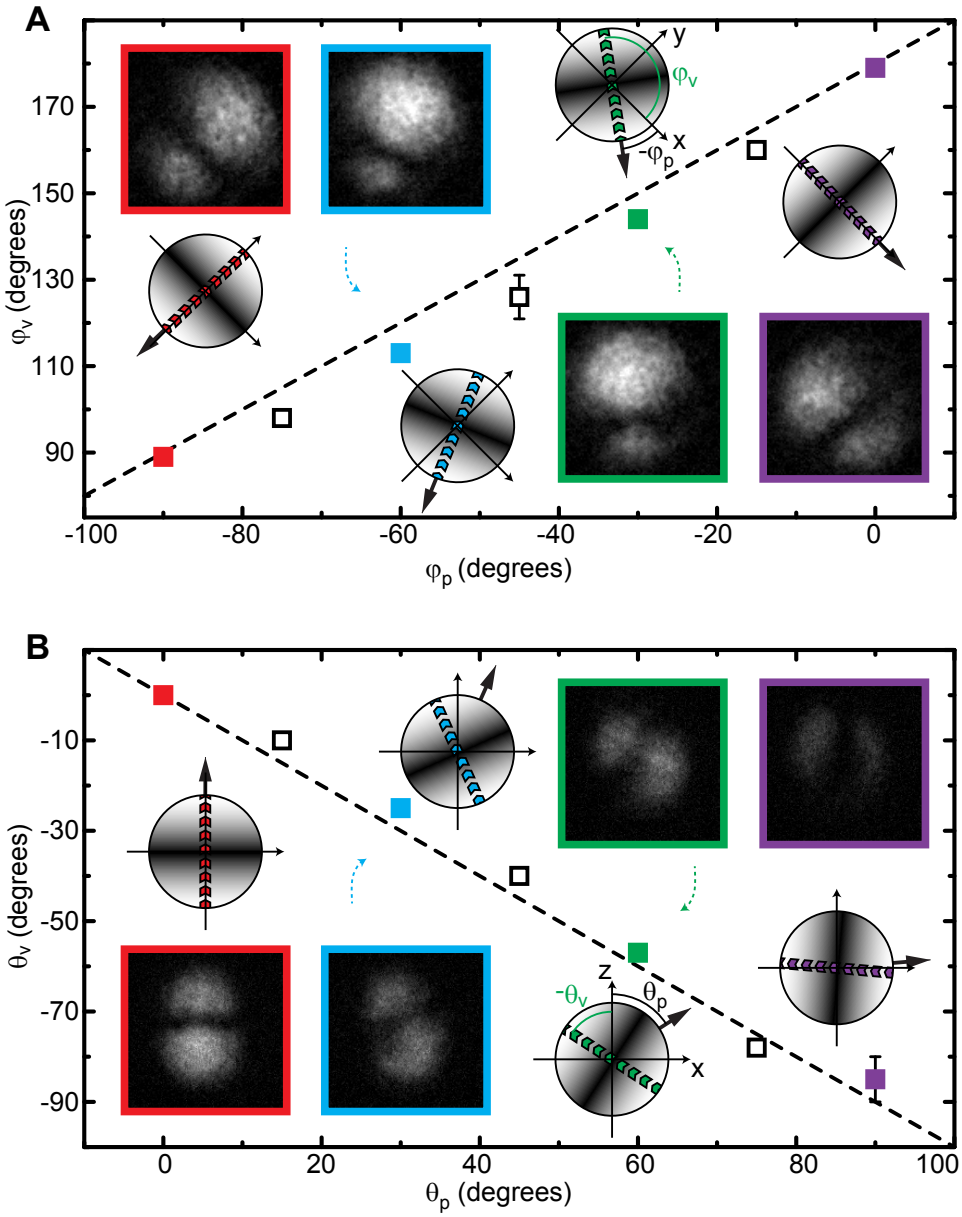

Fig. 4. Experimental results for different choices of the projection axis. (**A**) The angle of the vortices in the $|m = \pm 1\rangle$ states, φ_v, resulting from projections in the xy plane with azimuthal angle φ_p. Condensates are imaged along the z-axis and φ_v is extracted from the alignment of the density profile in the $|m = 0\rangle$ state as shown in the insets (see also Figs. S4-S7). Typical uncertainties are indicated by the two error bars. The dashed line shows the theoretical result. The black arrows in the insets show the projection axes, z_p, and the chevrons show the experimentally extracted vortex axes, z_v. (**B**) Same as (**A**) but for angles θ_v resulting from projections in the xz plane with polar angle θ_p and imaging axis y.